CHARACTERIZATION OF HYDROXY-INTERLAYERED VERMICULITE AND ILLITE/SMECTITE INTERSTRATIFIED MINERALS FROM THE WEATHERING OF CHLORITE IN A CRYORTHOD

DOMINIQUE RIGHI,[1] SABINE PETIT,[1] AND ALAIN BOUCHET[2]

[1] UA 721, CNRS, Laboratoires de Pédologie et Pétrologie de la Surface
Faculté des Sciences, 86022 Poitiers-Cedex, France

[2] ERM, Mérovée, BP25, 86320 Civaux, France

Abstract—X-ray diffraction, FTIR, and chemical analyses were performed on clay fractions (1–2 μm, <0.1 μm), separated by means of size fractionations and high-gradient magnetic separation techniques, from a Cryorthod developed in a chlorite-mica schist saprolite. Weathering of large phyllosilicates pre-existing in the saprolite involves physical fragmentation and mineralogical transformations. Chloritic minerals in the coarse fractions were the most affected by physical breakdown, while micas were generally preserved. As a consequence, a concentration of mica layers occurred in the coarse clay fraction, while chloritic residues accumulated in the fine clays. These residues exhibited the typical XRD pattern of hydroxy-interlayered intergrade minerals, but the interlayered contaminants were found to be mainly hydroxy-Mg cations. Further mineralogical transformations of the intergrade minerals involved the progressive removal of the hydroxide interlayered sheet and dissolution of chloritic layers. Illite/smectite mixed-layers were formed in the surface horizon of the soil profile. These processes were associated with a strong decrease in Fe and Mg contents in the clay fractions.

Key Words—Chlorite, Hydroxy-interlayered intergrades, Illite/smectite mixed-layers, Soil clays, Spodosol.

INTRODUCTION

Simple transformation of mica is the process most often described for the formation of soil clays, especially soil vermiculite and smectite (Borchardt, 1989; Douglas, 1989). In weakly acid soils, these clay minerals would be affected by hydroxy-interlayering, which is responsible for their intergrade behavior when subjected to XRD analysis (Barnhisel and Bertsch, 1989). However, saprolite of crystalline rocks, as well as loessial materials from which many typical temperate soils have developed, commonly contain chlorite as primary minerals. Although less abundant than mica, these minerals should not be disregarded because they are easily weatherable and an important possible source for soil clays, especially during the early stages of pedogenesis.

Although DeConinck et al. (1983) has interpreted most of the intergrade minerals in acid soils as weathering products of chlorite rather than hydroxy-Al interlayered vermiculite and smectite, studies on the weathering of chlorite in temperate acid soils are scarce (Bain, 1977; Churchman, 1980; Ross et al., 1982; Adams and Kassim, 1983) and the characterization of its weathering products is not well documented, especially their X-ray diffraction (XRD) behavior. The difficulty in characterizing such chloritic minerals lies mainly in the inability to separate or isolate them from the natural mixture of clays in which they occur.

The aim of this paper was to separate and charac-terize weathering products of chlorite from soil clays, using size fractionation followed by high gradient magnetic separation (HGMS). Particle size fractionation helps to isolate large inherited mineral grains from their weathering products, generally of a smaller size. HGMS concentrates minerals on the basis of their Fe content and generally is an efficient tool for the separation of chloritic minerals (Ghabru et al., 1990; Weed and Bowen, 1990).

SOIL MATERIAL

Clays were separated from a lithic, humic Cryorthod (Soil Taxonomy, USDA, 1986) or ochric podzosol (Référentiel Pédologique, INRA, 1992) developed from a chlorite-rich mica schist saprolite. The soil is from the Himalayas (Nepal) and located at the Matchembo pass at an elevation of 4020 m above sea level. A detailed description of this soil was given in previous papers (Righi and Lorphelin, 1986, 1987). Selected analytical data are listed in Table 1. Only a brief description is given below:

0–5 cm: A1. Dark reddish brown (5YR 2/2) silt loam, organic rich, strong fluffy structure, very friable, many fine roots, abrupt wavy boundary.

5–10 cm: A1/E. Reddish gray (5YR 5/2) silt loam, moderate fine subangular blocky structure, friable, many roots, clear broken boundary.

10–15 cm: Bh. Reddish brown (5YR 4/4) silt loam, moderate medium subangular blocky and fine gran-

484

Table 1. Analytical data for the soil (% 105°C dry soil) from Matchembo Pass.

Horizon	Depth cm	Clays %		OM %	pH H₂O	Al₂O₃ ox %	Fe₂O₃ ox %
		<2 μm	<0.1 μm				
A1	0–5	—	—	25.9	4.9	—	—
A1/E	5–10	17.1	4.6	18.0	4.5	0.6	1.5
Bh	10–15	13.1	4.1	11.1	4.6	1.1	4.1
Bw	15–20	9.5	2.4	5.6	4.8	1.1	3.4
C	>20	5.6	1.8	0.9	5.0	0.3	0.5

OM = organic matter.
Ox = oxalate extractable Fe and Al.

Table 2. Citrate-bicarbonate-dithionite extractable Al_2O_3 and Fe_2O_3 from the various fractions (% 105°C dry fraction).

Fraction		Fe₂O₃ %	Al₂O₃ %
A1/E	0–1 μm	10.4	1.1
	1–2	5.3	0.4
	2–5	3.1	0.1
	5–10	1.2	0.0
	10–20	1.2	0.0
Bh	0–1 μm	17.7	1.9
	1–2	15.0	1.0
	2–5	2.7	0.5
	5–10	2.2	0.5
	10–20	4.5	0.1
Bw	0–1 μm	15.4	3.1
	1–2	13.3	1.5
	2–5	6.2	0.4
	5–10	2.3	0.2
	10–20	2.0	0.1
C	0–1 μm	8.4	4.1
	1–2	5.0	2.0
	5–10	3.4	0.4
	10–20	0.9	0.1

ular structure, friable, many roots, clear wavy boundary.

15–20 cm: Bw. Dark brown (7.5YR 4/4) silt loam, weak medium and fine granular structure, friable, few roots, clear wavy boundary.

20–40 cm: C. Yellowish brown (10YR 5/4) loam, gravelly, no roots.

The soil has developed from a homogeneous parent material derived from the weathering of chlorite-rich mica schist and exhibits typical podzolization features. Podzolization has induced the most advanced transformation of the primary minerals, as compared with that in other soils of the area (Righi and Lorphelin, 1986).

SEPARATION AND ANALYTICAL METHODS

The clay and the silt fractions were obtained from the horizon samples by sedimentation after destruction of organic matter with diluted, Na-acetate buffered H_2O_2 (pH = 5) and dispersion in NaOH at pH = 9. The silt (2–5, 5–10, and 10–20 μm) and clay (<1, 1–2 μm) fractions were then treated with citrate-bicarbonate-dithionite (CBD) to remove crystalline and amorphous iron oxides and oxyhydroxides (Mehra and Jackson, 1960), especially those associated with the phyllosilicate surfaces that would interfere with the magnetic separation. However, that treatment may induce slight alteration of some Fe-bearing silicates (Douglas, 1967) and partial dissolution of smectites (Stucki et al., 1984).

The <1 μm deferrated clay fraction was divided into <0.1, 0.1–0.2, and 0.2–1 μm subfractions by centrifugation using a Beckman J2-21 centrifuge equipped with the JCF-Z continuous flow rotor. The clay subfractions were then subjected to high gradient magnetic separation (HGMS) according to the method of Righi and Jadault (1988). A magnetic fraction (M), retained on the magnetic filter in a magnetic field of 2 T, and a non-retained tail fraction (N) were collected. The silt sub-fractions were separated using two values of magnetic field, 0.2 and 2 T; resulting in the collection of two sub-samples, a weakly and a strongly magnetic one.

X-ray diffraction (XRD) diagrams were obtained from parallel-oriented specimens using a Philips dif-fractometer with Fe-filtered $CoK\alpha$ radiation. Pretreatment of the specimens included Ca saturation and solvation with ethylene glycol and K saturation followed by heating to 110, 300 and 550°C. The diffractograms were recorded numerically by a DACO-MP recorder associated with a microcomputer using the Diffrac AT software (SOCABIM, France). The XRD diagrams were then decomposed into their elementary component curves using the least-squares computer program of Lanson and Besson (1992). Such a decomposition allowed an improved measure of the position and relative intensity of the diffraction peaks. Simulated diagrams made with the NEWMOD program of Reynolds (1985) were also used to help interpretation of experimental XRD diagrams. High-charge and low-charge smectite layers were identified on the basis of re-expansion with ethylene glycol after K-saturation and heating to 110°C. The Greene-Kelly (1953) test (Li saturation) was used to distinguish montmorillonite and beidellite.

The Na-citrate treatment (Tamura, 1958) was used to extract hydroxy-Al interlayered polycations. The extract was analyzed by atomic adsorption spectroscopy (AAS).

FTIR spectroscopy was performed on KBr disks prepared by mixing 1 mg sample with 300 mg KBr and pressing at 13 kg/cm². FTIR spectra were recorded using a Nicolet 5DX spectrometer.

Total analyses were performed on CBD treated samples according to procedure described by Jeanroy (1972). Si, Al, Fe, Ti, Mg, Ca, Na, and K were analyzed by AAS.

Cation exchange capacity (CEC) was obtained from the CBD treated samples by saturation with Mg^{2+}, the
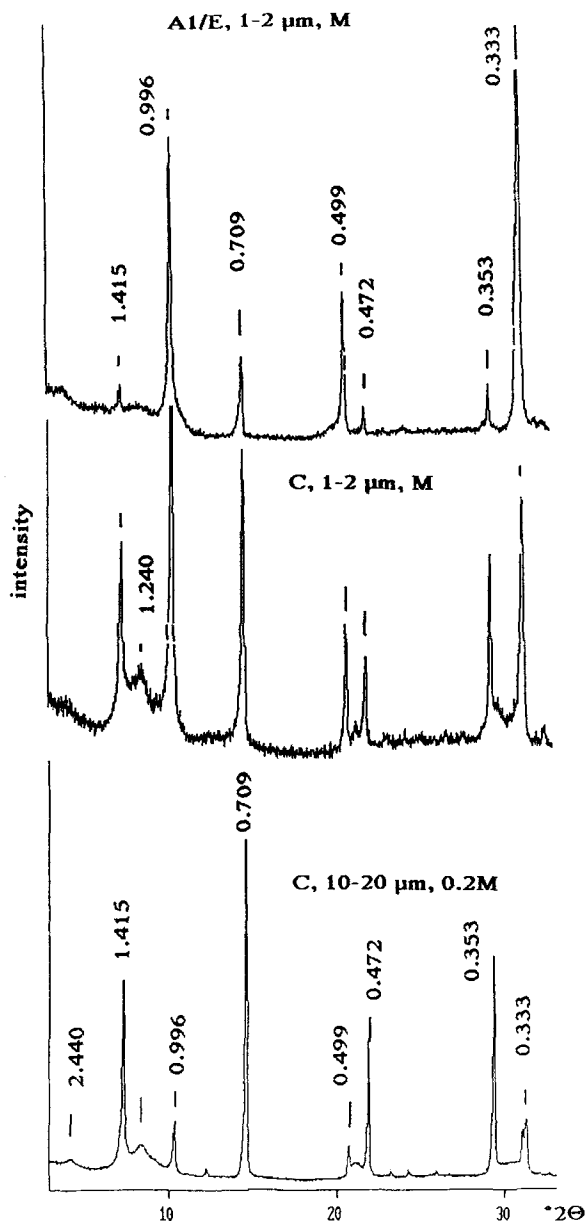
Figure 1. XRD diagrams for magnetic (M) silt and coarse clay fractions (Ca saturated, ethylene glycol solvated) from the C and A1/E horizons. CoKα radiation, d-spacings in nm.

excess of Mg salt ($MgCl_2$) being carefully washed out with ethanol. Mg^{2+} was then exchanged by N,NH_4^+ and analyzed by AAS in the exchange solution.

RESULTS AND INTERPRETATION

Total clay (<2 µm) increased from 0.56 g/kg in the C horizon to 1.73 g/kg in the A1/E horizon, where the fine fractions (<0.2 µm) were 0.18 g/kg and 0.46 g/kg respectively (Table 1).

The CBD-extracted Fe and Al, expressed as Fe_2O_3 and Al_2O_3, are given in Table 2. These amounts de-

creased with the increase of particle size. Extractable Fe_2O_3 was the largest in the Bh and Bw horizons, and maximum extractable Al_2O_3 was found in the lowest part of the soil profile (Bw and C horizons). Such a depth distribution is typical for a Spodosol.

Ratios for the magnetic (M) to the non-magnetic (N) fractions were not quantified but the tendency was to find increasing amounts of N in the <0.1 µm fraction from the C to the A1/E horizons.

Mineralogy of the silt and coarse clay fractions

The silt fractions retained on the magnetic filter for an applied magnetic field of 2.0 or 0.2 T were analyzed by XRD. All the samples exhibited the reflections of chlorite (d = 1.415, 0.706, 0.470, and 0.353 nm) and mica (d = 0.996, 0.498, and 0.333 nm) (see Figure 1). Additional reflections at d = 0.124 and 0.482 nm were attributed to mica/vermiculite interstratified minerals. Heat treatments (550°C) induced a decrease of the reflection at d = 1.415 nm with a parallel increase of that at 0.996 nm that was indicative of vermiculite layers. Reflections at d = 0.156 and 0.154, 0.152 nm (not shown) were attributed to chlorite and trioctahedral minerals respectively.

The XRD diagrams from the 2.0 and 0.2 M fractions were very similar, except for the relative intensities of the chlorite and mica reflections. The 0.2 M fraction contained more chlorite than the 2.0 M fraction which was mica-rich, and identical to the M coarse clay (1–2 µm) fraction from the C horizon (Figure 1).

From the C to the A1/E horizons, the M coarse clay fraction was characterized by a decrease of the intensities of the reflections from chlorite and intergrade minerals. The M coarse clay fraction from the A1/E sample was almost exclusively composed of a mica with a small amount of chlorite (Figure 1). The 060 reflection at d = 0.150 nm (not shown) indicated that the mica from the A1/E horizon sample was dioctahedral.

Heat treatment (550°C) on the coarse clay samples induced a decrease of the reflection at d = 1.415 nm, with a parallel increase of that at 0.996 nm and the disappearance of the reflection at d = 1.240 nm, which was indicative of vermiculite layers. However, the decomposition of the peak at d = 0.996 nm gave three basic curves, one of these sharp (maximum at d = 0.996 nm) and the others, broad and weak with a maximum at higher d-spacings, indicating uncollapsed layers that could be attributed to interstratified chlorite (Figure 2). Moreover, the collapse of the coarse clay was obtained progressively as the heating temperature increased, leading to a typical intergrade behavior. Such a behavior was attributed to an incomplete hydroxide interlayered sheet (Barnhisel and Bertsch, 1989). These uncollapsed layers were less abundant in the A1/E coarse clay than in the C coarse clay sample.

Mineralogy of the fine clay fractions

General. No major differences were observed between the M and N subfractions; thus, only the results from the N subfractions are given below, the N subfraction being the most abundant. Compared with the N subfractions, M samples exhibited only slightly larger proportions of chlorite layers.

All the <0.1 μm fractions were composed primarily of dioctahedral minerals as indicated by the 060 reflection at d = 0.150 nm (not shown).

The fine clay fractions (<0.1 μm) from the C horizon were not abundant enough to be separated by HGMS; thus, the whole <0.1 μm fraction was used for XRD. Except for some smectite layers, this fraction gave an XRD diagram identical to that of the coarse clay fraction. Especially, the behavior after K-saturation and heating was identical.

Bw horizon sample. For the Bw, <0.1 μm N fraction, the decomposition of the XRD diagram from the glycolated sample in the 6–12° 2Θ region gave three basic curves with maximum intensities at d = 1.422, 1.305 (broad) and 1.021 nm (Figure 3). That fraction was also characterized by a very strong relative intensity of the reflection in the 18–23° 2Θ region, which was decomposed into two basic curves of quite equal intensities with their maxima at d = 0.495 and 0.480 nm (Figure 3). Four basic curves were required in the 28–33° 2Θ region: three rather sharp curves with their maxima at d = 0.357, 0.352, and 0.334 nm and a broader one with its maximum at d = 0.345 nm (not shown).

The peak at d = 1.422 nm was attributed to vermiculite and chlorite (associated with the peak at d = 0.352 nm). The peaks at d = 0.720 nm and d = 0.357 nm were attributed to kaolinite. Simulated XRD patterns were made with the NEWMOD program (Reynolds, 1985) in order to better characterize the other mineral phases.

According to Reynolds (1980), only illite/chlorite interstratified minerals give an intense reflection in the 18–23° 2Θ (0.50–0.47 nm) region, as was observed in the Bw, <0.1 nm N sample. The position of the peak moves from 0.501 to 0.473 nm with increasing proportion of the chlorite component, but that position is sensitive to the size of the coherent scattering domain (CSD), and it shifts toward higher d-spacings as CSD size decreases. Also the width of the peak is affected: it increases as CSD size decreases. Relative to that of the first order reflection (in the 1.00–1.40 nm region), the intensity of the peak near 0.50 nm is strongly decreased when the hydroxide sheet of the chlorite component is not complete.

The simulated XRD pattern of illite/chlorite mixed-layers with 40% illite (Figure 4) gave three peaks at d = 1.318, 0.480, and 0.347 nm that matched reasonably well with the experimental reflections at d = 1.305,
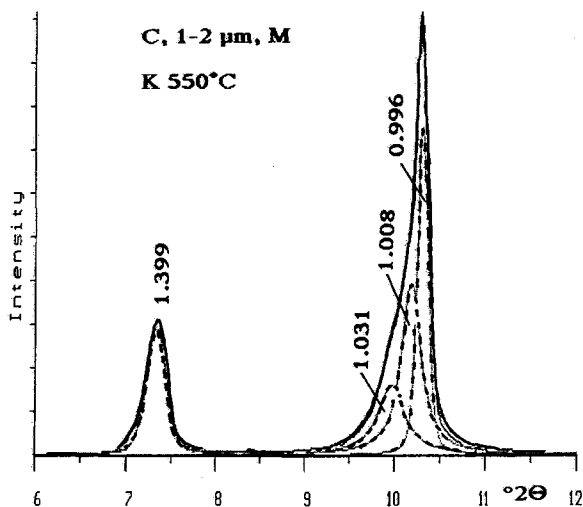

Figure 2. Decomposed XRD diagram for the magnetic (M) coarse clay fraction from the C horizon, K-saturated and heated to 550°C. CoKα radiation, d-spacings in nm. (– – –) = computed elementary curves; (——) = experimental curve; (━━) = best-fit computed curve.

0.480, and 0.345 observed for the Bw, <0.1 nm N sample. As experimental reflections were also found at d = 1.021, 0.495, and 0.334 nm, a good agreement was observed with another simulated illite/chlorite mixed-layers with 90% illite, giving peaks at d = 1.023, 0.495, and 0.334 nm (Figure 4). For these two simulated illite/chlorite, the width and relative intensity of the 2nd and 3rd order peaks also matched well with the experimental data. Only the width of the 1rst order peaks (d = 1.318, 1.021 nm) were far narrower in the simulated diagrams than in the experimental patterns. This peak width problem, in that angular range, was also reported by Lanson and Besson (1992) for illite/smectite mixed-layers. Thus, decomposition of the XRD diagram, with the help of simulated patterns, allowed identification of two illite/chlorite mixed-layers: one illite-rich with 90% illite, the other chlorite-rich with 60% chlorite.

Following heat treatments, the XRD pattern from the Bw, <0.1 μm N fraction showed a very strongly expressed intergrade character (Figure 3). Collapse of the interlayers was very progressive and far from complete, leading (after heating at 550°C) to a strongly asymmetrical reflection. In the 6–12° 2Θ region, the diagram was decomposed into three basic curves with their maxima at d = 1.370, 1.137 and 1.019 nm. The first peak was attributed to chlorite. The most intense peak was at d = 1.137 nm and broad. It was interpreted as an interstratification of collapsed and uncollapsed layers, as was the third peak at d = 1.019 nm, but the proportion of uncollapsed layers was lower in that case.

After the Na-citrate treatment, the treated sample, K-saturated and heated to 550°C, still gave an asymmetrical reflection (Figure 3). However, changes in the
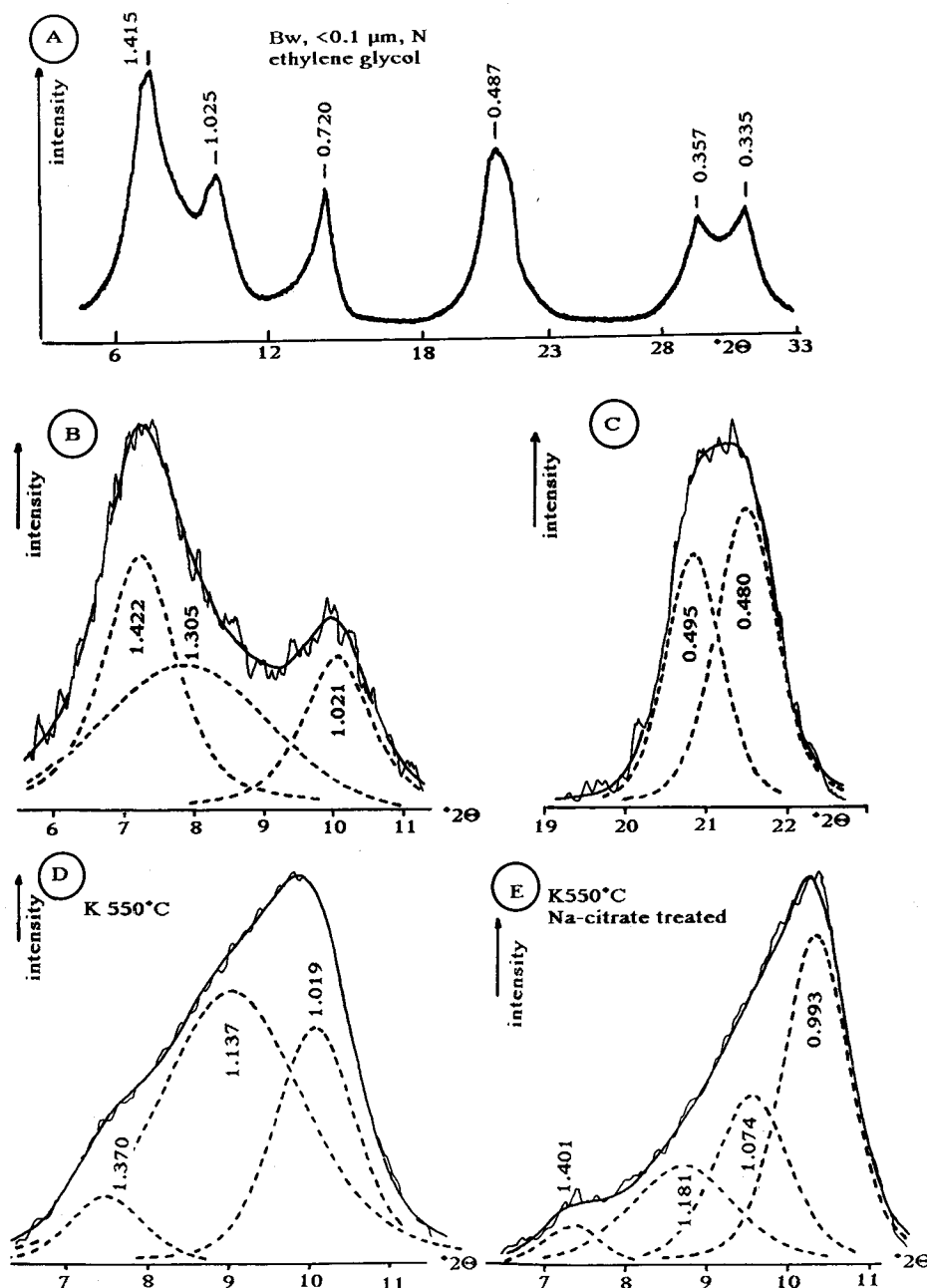
Figure 3. XRD diagrams for the non magnetic (N) fine clay fraction from the Bw horizon. CoKα radiation, d-spacings in nm: A) experimental diagram, Ca saturated, ethylene glycol solvated; B) decomposed diagram in the 5–12° 2Θ region, Ca saturated, ethylene glycol solvated; C) decomposed diagram in the 18–23° 2Θ, Ca saturated, ethylene glycol solvated; D) decomposed diagram in the 5–12° 2Θ region, K-saturated and heated to 550°C; E) decomposed diagram in the 5–12° 2Θ region, Na-citrate treated, K-saturated and heated to 550°C. (− − −) = computed elementary curves; (———) = experimental curve; (▬▬) = best-fit computed curve. Intensity scale is not identical for B, C, D and E.

relative intensities of the basic curves were observed. After the treatment, the most intense peak was found at d = 0.993 nm, but a peak at d = 1.401 nm was still present. The peak at d = 0.993 nm was attributed to collapsed vermiculite layers. In the 18–23° 2Θ region,

peaks at d = 0.475 nm and 0.490 nm were observed, indicating that chlorite and illite/chlorite were still present after the citrate treatment (not shown). However, the peak at 0.480 nm was not maintained for the treated sample. Also the relative intensity of the peak
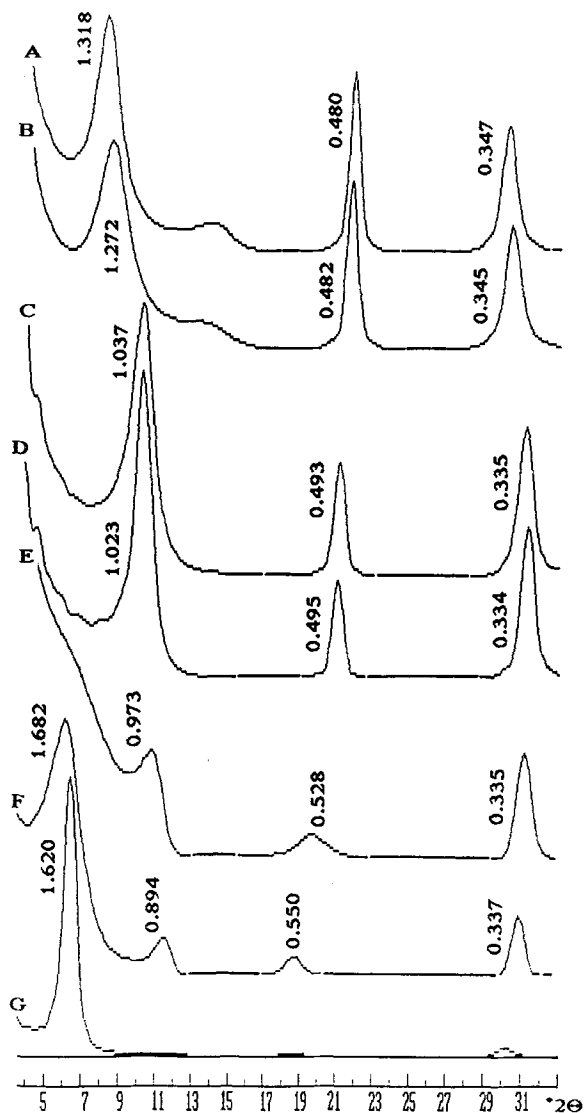
Figure 4. Simulated XRD diagrams using NEWMOD program: A) illite/chlorite, random, 40% illite; B) illite/chlorite, random, 50% illite; C) illite/chlorite, random, 85% illite; D) illite/chlorite, random, 90% illite; E) illite/smectite, random, 72% illite; F) illite/smectite, random, 40% illite; G) vermiculite/smectite, random, 40% vermiculite. Coherent scattering domain size: 10–15 layers.

at d = 0.475 nm in the treated sample was strongly decreased as compared with the 0.480 nm peak in the untreated sample. Although some vermiculite layers have been produced during that treatment, it appeared that the Na-citrate treatment did not greatly improve the collapse of the interlayers. The mineral phase most affected by the treatment was the chlorite-rich, illite/chlorite interstratified mineral, but chlorite was only slightly affected.

Mg, Fe, and Al were analyzed in the extract (Table 3). Mg was far more extracted than Al as indicated by the Al/Mg atomic ratios in the extract (Al/Mg = 0.77). Extracted amounts of K and Si indicated complete dissolution of some layers, including illite.

Bh horizon sample. For the Bh, <0.1 μm N fraction, the decomposition of the XRD diagram in the 6–12° 2Θ region gave four basic curves with their maxima at d = 1.423, 1.270, 1.036, and 1.624 nm (Figure 5). In the 18–23° 2Θ region, two peaks were obtained at d = 0.493 and 0.482 nm (Figure 5), and three peaks were observed at d = 0.357, 0.345, and 0.335 nm (not shown) in the 28–33° 2Θ region.

The peak at 1.423 nm was attributed to vermiculite. The peak at d = 0.357 nm in the 28–33° 2Θ region was taken as evidence of kaolinite layers. As for the Bw sample and according to simulations with the NEWMOD program (Figure 4), the peak at d = 1.270 nm, associated with those at d = 0.482 and 0.345 nm, was attributed to illite/chlorite mixed-layers with 50% chlorite. The peak at d = 1.036 nm associated with those at d = 0.493 and 0.335 nm matched well with the simulated pattern of illite/chlorite mixed layers with 85% illite (Figure 4). The peak at d = 1.624 nm could be simulated either by chlorite/smectite or vermiculite/smectite mixed layers with 40% of vermiculite or chlorite (Figure 4).

The Bh, < 0.1 μm N sample was K-saturated, heated to 110°C, ethylene glycol-solvated, and then subjected to XRD. Following that treatment, no swelling was observed (not shown), indicating that the smectite layers already identified in this sample were high-charge layers. Following the Greene-Kelly (1953) test, a swelling up to d = 1.70 nm was observed, thus indicating that at least part of the smectite layers were beidellite (Figure 6).

Table 3. Composition of Na-citrate extracts.

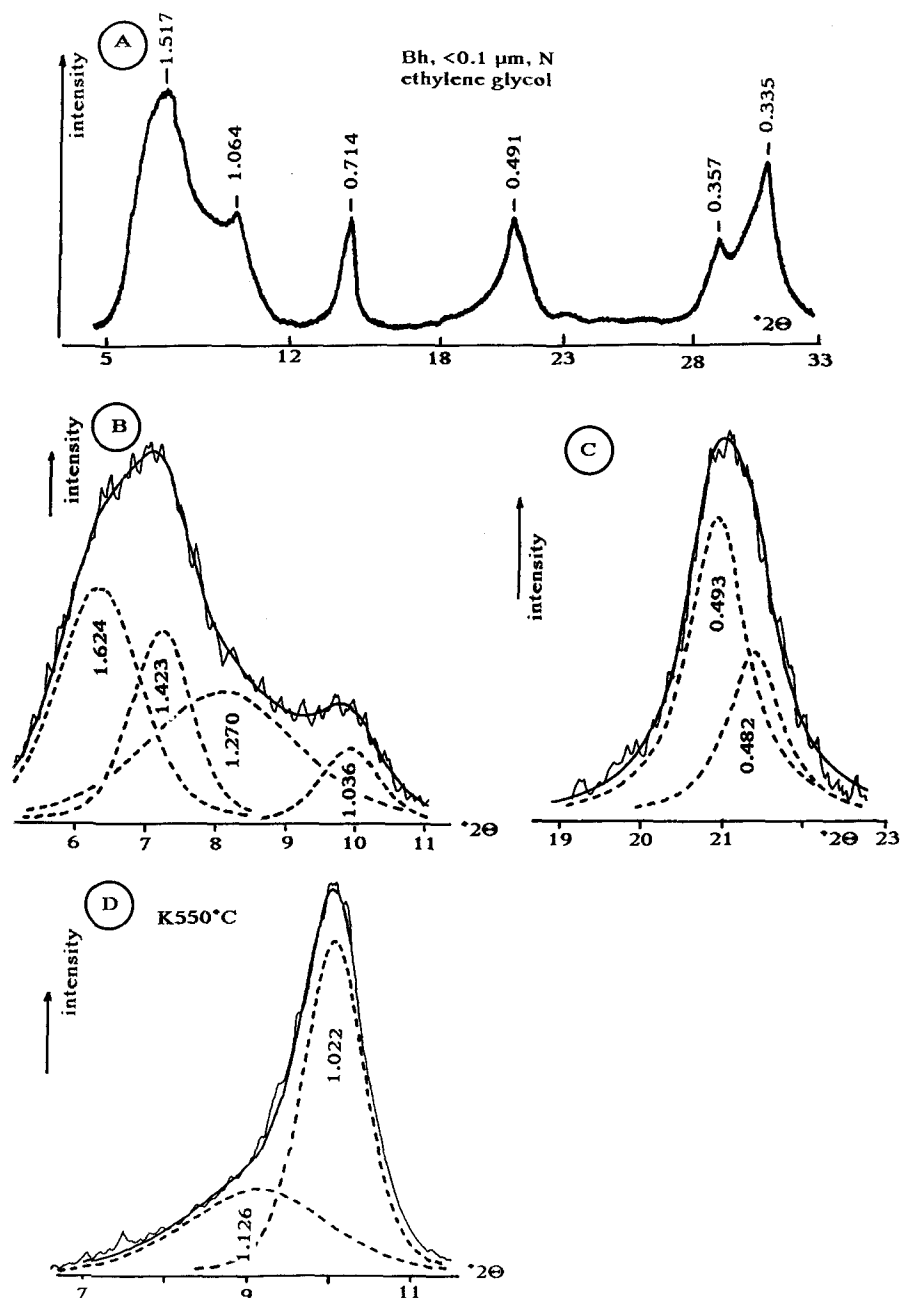| Sample	Al₂O₃ (1)	Al₂O₃ (2)	Fe₂O₃ (1)	Fe₂O₃ (2)	MgO (1)	MgO (2)	K₂O (1)	K₂O (2)	SiO₂ (1)	SiO₂ (2)	Al/Mg*
Bh <0.1 μm, N	0.8	3.2	1.9	22.5	0.4	18.0	0.2	6.0	2.2	5.2	1.51
Bw	1.7	6.8	1.4	14.3	1.7	30.0	0.2	8.0	2.3	5.8	0.77

(1) % 105°C, dry sample.
(2) % Total oxide.
* Atomic ratio.

Figure 5. XRD diagrams for the non-magnetic (N) fine clay fraction from the Bh horizon, with CoKα radiation, d-spacings in nm: A) experimental diagram, Ca saturated, ethylene glycol solvated; B) decomposed diagram in the 5–12° 2Θ region, Ca saturated, ethylene glycol solvated; C) decomposed diagram in the 18–23° 2Θ, Ca saturated, ethylene glycol solvated; D) decomposed diagram in the 5–12° 2Θ region, K-saturated and heated to 550°C. (– – –) = computed elementary curves; (——) = experimental curve; (▬▬) = best-fit computed curve. Intensity scale is not identical for B, C and D.

In response to heat treatments, the collapse of the interlayers was obtained far more easily than for the Bw sample. Collapse was quite complete after heating at 300°C, and it led, after heating at 550°C, to a peak at d = 1.022 nm and to a broader one at d = 1.126 nm (Figure 5). Compared with the Bw sample, the proportion of uncollapsed layers in this sample was drastically decreased. After the Na-citrate treatment, the XRD diagram pattern was not changed, especially in the 18–23° 2Θ region for which the decomposition gave the same basic curves for either the treated or untreated sample.

In the Na-citrate extracts, lower amounts of Mg than in the extract from the Bw, <0.1 μm N fraction were analyzed (Table 3).

A1/E horizon sample. From the A1/E horizon, <0.1 μm N fraction, only three basic curves were obtained by decomposition in the 4–12° 2Θ region, their maxima being at d = 1.631, 1.384, and 0.985 nm (Figure 7). The peak at d = 0.985 nm was attributed to illite/smectite interstratified minerals and the peak at d = 1.384 nm to illite/vermiculite (or chlorite). The peak at d = 1.631 nm could be given by vermiculite/smectite mixed layers (60% smectite) or illite/smectite (60% smectite) as suggested by the NEWMOD simulations (Figure 4).

In the 18–23° 2Θ region, three peaks were obtained at d = 0.505, 0.527, and 0.551 nm and attributed to illite and illite/smectite interstratified minerals (Figure 7). According to the simulations, the two peaks at d = 0.527 and 0.551 nm indicated two types of illite/smectite mixed layer minerals: 1) d = 0.551 nm, with a high ratio of illite layers (72%); 2) d = 0.527 nm, with a lower ratio of illite layers (40%) (Figure 4). The peak at d = 0.505 nm indicated illite. A peak at d = 0.480 nm was present, indicating illite/chlorite mixed layers as in the previous samples. In the 28–33° 2Θ region, four peaks at d = 0.357 nm (attributed to kaolinite), d = 0.332 and 0.335 nm (attributed to illite and illite/smectite), and d = 0.355 nm (attributed to illite/vermiculite) were obtained (not shown). The peak at d = 0.344 nm, which was present in the Bw and Bh samples, has disappeared.

The A1/E, <0.1 μm N fractions were K-saturated, heated to 110°C, ethylene glycol-solvated, and then subjected to XRD. Following that treatment, no swelling was observed (not shown), indicating that the smectite layers were high-charge layers. In response to the Greene-Kelly (1953) test, no swelling was obtained. So, in the A1/E sample, smectite layers would be montmorillonite (Figure 6).

FTIR spectroscopy

Three main absorption bands were observed on the FTIR spectra in the 3800–3000 cm^{-1} region. The broad, poorly expressed band at about 3440 cm^{-1} was attributed to OH-stretching vibrations of hydroxide in the interlayer sheets (Makumbi and Herbillon, 1972; Senkayi *et al.*, 1981). The strongest band at 3630 cm^{-1} and the weaker one at 3700 cm^{-1} were assigned to OH-stretching in the octahedral sheet of aluminous minerals like mica or kaolinite.

The band at 3440 cm^{-1} was most intense and best defined in the C, 1–2 μm M sample, related to well organized brucite layers in this sample.

Although XRD showed far more interlayered material in the Bw, <0.1 μm N sample than in the Bh, <0.1 μm N sample, no obvious differences were ob-
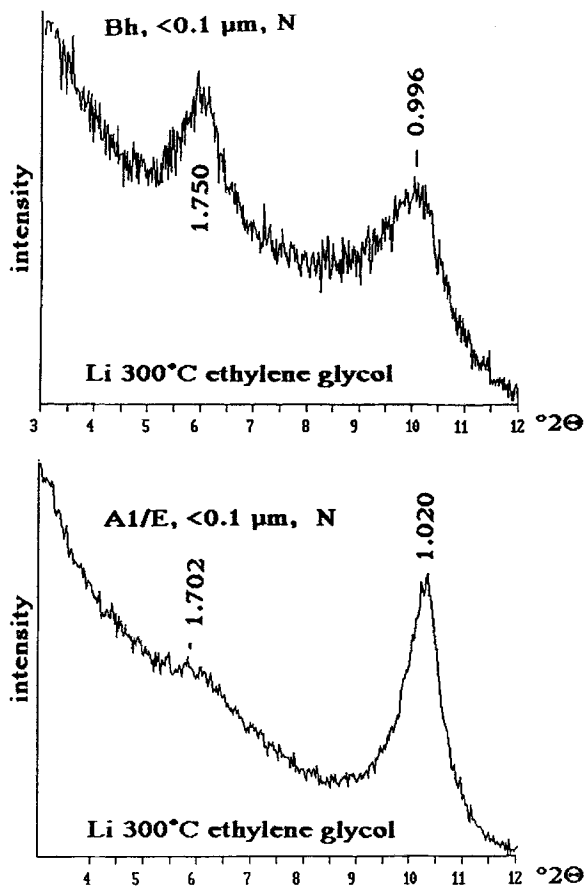

Figure 6.   XRD diagrams for the non-magnetic (N) fine clay fractions from the Bh and A1/E horizons. Experimental diagrams, Li saturated, heated to 300°C and ethylene glycol solvated. CoKα radiation, d-spacings in nm.

served on the FTIR spectra. The same features were observed by Senkayi *et al.* (1981) for experimentally altered chlorite and would be explained by assuming that the regularity of atomic ordering in the interlayered hydroxide sheet was greatly disturbed, leading to poorly defined IR adsorption bands.

Heating the KBr disk up to 500°C caused the band at 3700 cm^{-1} to disappear (this was attributed to kaolinite) and to the improvement of the 3440 cm^{-1} band. Further heating to 600°C induced the disappearance of the 3630 cm^{-1} band, but that at 3440 cm^{-1} was preserved. The low thermal stability of 2:1 mica layer (3630 cm^{-1}) was attributed to a rather high ratio of Fe in the octahedral sheet. From the greater thermal stability of the hydroxide sheet, it was concluded that it was mainly magnesian (Caillère and Hénin, 1960). Only the A1/E, <0.1 μm N sample did not exhibit any absorption band after heating to 600°C, which was in agreement with the XRD results showing only very small amounts of interlayered material in this sample (Figure 8).
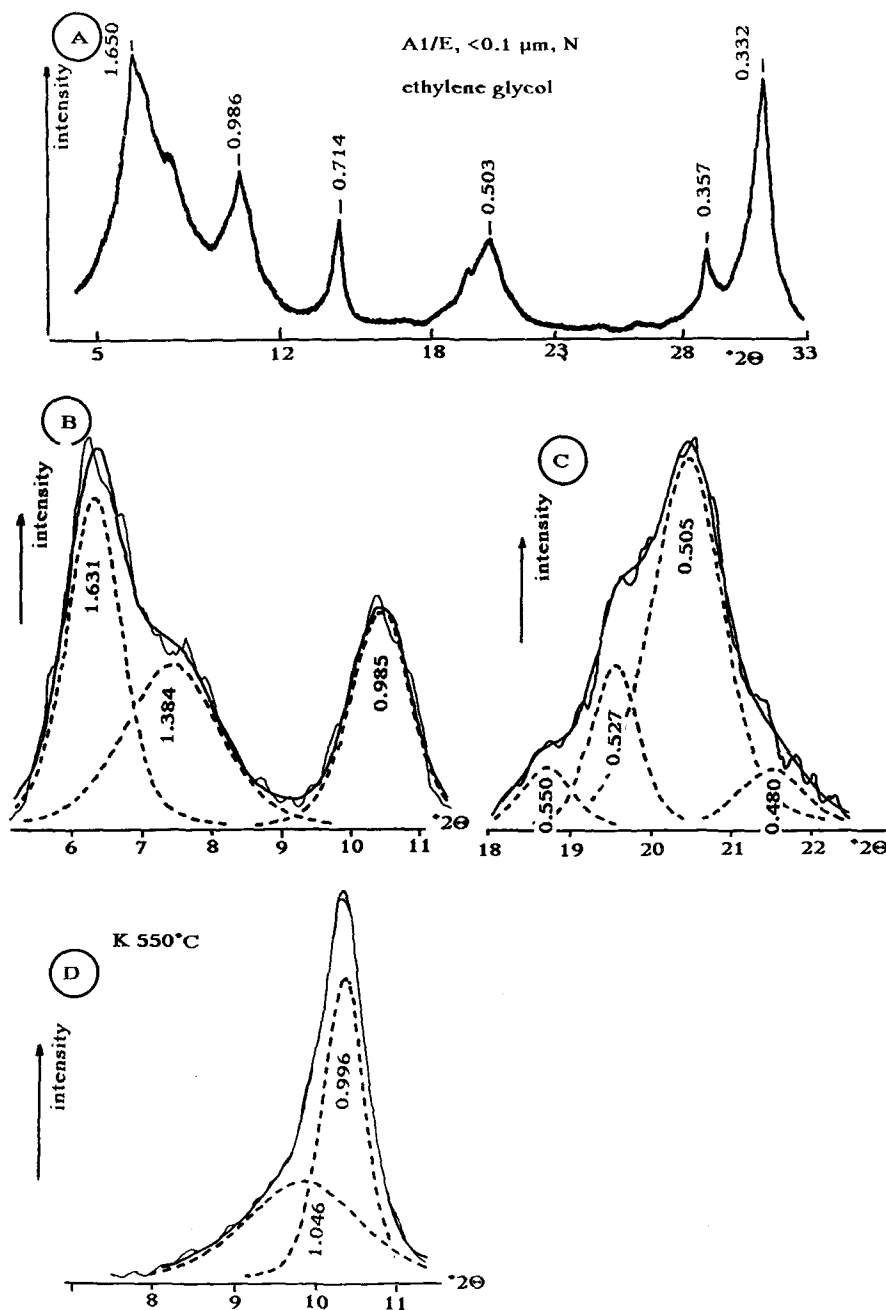
Figure 7.   XRD diagrams for the non-magnetic (N) fine clay fraction from the A1/E horizon, with CoKα radiation, d-spacings in nm: A) experimental diagram, Ca saturated, ethylene glycol solvated; B) decomposed diagram in the 5–12° 2Θ region, Ca saturated, ethylene glycol solvated; C) decomposed diagram in the 18–23° 2Θ, Ca saturated, ethylene glycol solvated; D) decomposed diagram in the 5–12° 2Θ region, K-saturated and heated to 550°C. (– – –) = computed elementary curves; (——) = experimental curve; (▬▬) = best-fit computed curve. Intensity scale is not identical for B, C and D.

The same heat treatment (500°C) was applied on Na-citrate treated samples. Compared with the untreated samples, no obvious differences were shown. It was concluded that the Na-citrate treatment did not selectively extract interlayered materials, especially if they are Mg-hydroxide.

Cation exchange capacity

The highest CEC (65 and 68 cmol$_c$/kg) (Table 4) was obtained for the Bw, <0.1 and 0.1–0.2 μm N fractions, in spite of large amounts of interlayered contaminants. Moreover, the same CEC was found for the A1/E, <0.1

μm N sample, which exhibited far less interlayering. CECs were shown to be decreasing with increasing particle sizes. The strong correlation between CEC and the K_2O content observed in a previous study (Righi and Meunier, 1991) was not found here. That agrees with the fact that, for the present samples, the CEC value is controlled by the proportion of illite, chlorite, vermiculite, and smectite—and not only by illite and vermiculite or smectite as in the previous study.

Total chemical analysis

Total chemical analysis of some selected fractions are given in Table 5. The 0.2 T magnetic fraction which is mainly chloritic showed larger amounts of Mg and Fe and lower amounts of K than the 2 T magnetic fraction, which is mica-rich. The composition of the C, 1–2 μm M sample was intermediate between these two extremes. Compared with the C horizon coarse clays, those from the A1/E horizon showed strongly decreased amounts of Mg and Fe, but K was not relatively increased as one would have expected from the XRD data indicating relative concentration of mica in this sample.

For the fine clay samples (<0.1 and 0.1–0.2 μm) the most important feature was the strong decrease in the Mg content from the Bw to the Bh and A1/E samples. For the coarse clays (1–2 μm), the decrease in the Mg content was observed from the C to the Bw sample, which agreed with the decrease of chlorite as shown by XRD. The K_2O content increased from the Bw, <0.1 μm N to the A1/E, <0.1 μm N fraction, indicating increasing proportions of illite layers.

DISCUSSION

The silt and coarse clay magnetic fractions from the C horizon contained a mixture of chlorite and mica layers that were not possible to separate completely by HGMS because these two minerals are probably partly associated in the same particles. A third mineral phase was also collected from the coarse clays: a randomly interstratified mica/chlorite mineral for which the heat treatment indicated a low thermal stability of the chlorite component. Such a low thermal stability could be related to an incomplete hydroxide sheet (Barnhisel and Bertsch, 1989).

For the coarse clays (1–2 μm) the major change from the C to the A1/E horizon was the decrease of the proportion of the chlorite and mica/chlorite components. The A1/E horizon coarse clay was almost exclusively constituted of mica layers. This demonstrated the preferential physical fragmentation of chlorite and mica/chlorite particles leading in the concentration of more resistant mica layers in the coarse clay fractions. The same was observed in the pedogenic weathering of clays in a soil developed in a granitic saprolite (Righi and Meunier, 1991). In good agreement was the de-
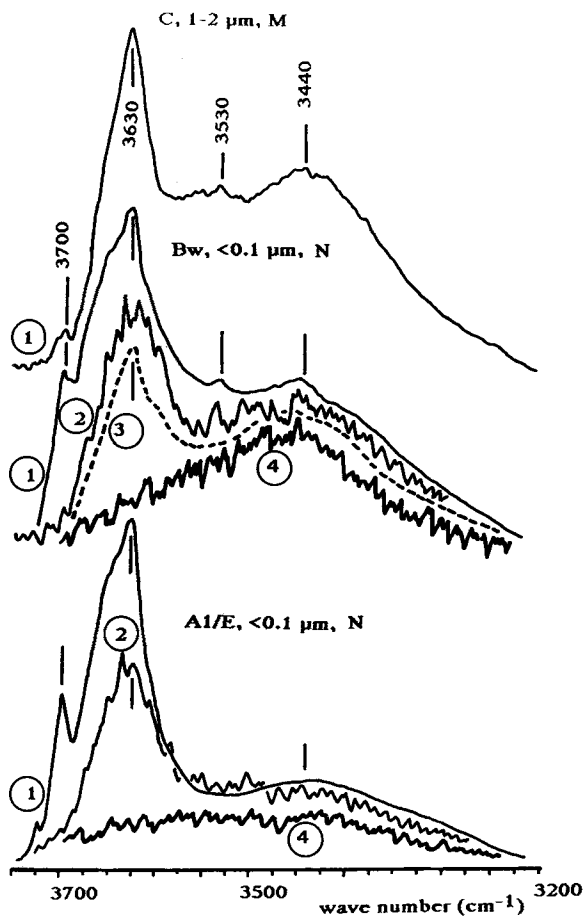

Figure 8. FTIR spectra for some selected clay fractions: 1) K-saturated sample; 2) 500°C heated KBr disk; 3) Na-citrate treated sample, 500°C heated KBr disk; 4) 600°C heated KBr disk.

crease of the 0.154 nm XRD reflection intensity (trioctahedral minerals) from the C to the A1/E samples.

The decrease in Mg and Fe content is also well explained by the preferential weathering of the Fe, Mg-rich chloritic layers. Although mica layers were relatively accumulated in the A1/E horizon sample, the K content was not strongly increased in this sample, this would indicate K-depletion of the mica (vermiculitization). The rather large amounts of CBD-extractable iron indicated that the release of iron from the Fe, Mg-rich phyllosilicates and its subsequent precipitation as amorphous and/or crystalline oxides are important steps of the weathering process.

The Bw fine fraction (<0.1 μm, N) was dominated by minerals with a strongly expressed XRD intergrade behavior. So, the greatest concentration of hydroxy-interlayered minerals was found in the fine clay fraction from the Bw, a sub-surface horizon, but not in the A1/E horizon, a fine clay sample. This was in disagreement with the results of Weed and Bowen (1990), who stated

Table 4. Cationic exchange capacity of selected fractions (cmol$_c$/kg, 105°C dry sample).

Sample	CEC	Sample	CEC	Sample	CEC
A1/E		Bh		Bw	
1–2 µm, M	11.0	1–2 µm, M	21.6	1–2 µm, M	17.5
0.1–0.2 µm, N	42.4	0.1–0.2 µm, N	32.1	0.1–0.2 µm, N	68.2
<0.1 µm, N	57.6	<0.1 µm, N	48.2	<0.1 µm, N	65.5

that maximum concentration of hydroxy-interlayered minerals would be found in the surface horizon and in the coarse clays.

The intergrade XRD behavior is generally attributed to hydroxy-Al interlayered polycations (Barnhisel and Bertsch, 1989), which can be removed by the Na-citrate treatment. In the present study, the Na-citrate treatment did not actually improve the collapse of the intergrade minerals. Moreover, the Na-citrate extract was rich in Mg, especially for the Bw, <0.1 µm N sample. This is a strong indication that, in the present case, interlayered materials are not aluminous but mostly magnesian. Another confirmation was given by FTIR spectroscopy showing a hydroxide interlayered sheet stable upon heating up to 600°C. Such a thermal stability is related to a hydroxide sheet with Mg as the dominant cation. Ghabru *et al.* (1990) also reported an intergrade hydroxy-interlayered vermiculite in which the interlayered contaminant was not Al but Fe cations.

From the Bw to the Bh and A1/E horizons, these intergrade minerals were progressively transformed into interstratified minerals that included a smectitic component. These appeared to be randomly interstratified chlorite/smectite or vermiculite/smectite minerals in the Bh horizon and illite/smectite in the A1/E horizon. Decreasing abundance of interlayered material was shown by the decrease of the relative intensity of the XRD reflection in the 0.50 nm region, in good agreement with the improved collapse of the minerals in response to heat treatments. Thus a decrease in the proportion of chlorite layers (or layers with interlay-

ered contaminants) was observed in the fine clays from the bottom to the top of the soil profile. In good agreement with the XRD diagram patterns was the chemical composition of these fine clay fractions: from the Bw to the A1/E horizon, a decrease in the Mg and Fe contents was observed with a parallel increase in the K content.

The smectitic component of these interstratified minerals appeared to be first beidellitic (tetrahedral charge) in the Bh and then montmorillonitic (octahedral charge) in the A1/E horizon. Proust *et al.* (1986) made a similar observation and stated a decrease of the Al-for-Si tetrahedral substitutions with chlorite weathering.

The illite/smectite interstratified minerals that were found in the A1/E horizon might come from either the transformation of the chlorite and illite/chlorite mixed-layers present in the lower horizons through the preferential dissolution of the brucite sheet or from the transformation of illite or mica through exchange of K for hydrated exchangeable cations. The first possibility is supported by the suspected formation of chlorite/smectite interstratified mineral in the Bh horizon and by illite/chlorite mixed layers associated with the illite/smectite in the A1/E horizon. If this is true, one must assume that part of the smectite layers has finally dissolved in order to explain the increase in K content in the A1/E, <0.1 µm N sample, indicating a higher proportion of illite layers. The formation of illite/smectite through transformation of illite is also a possibility, K-depletion in the mica from the 1–2 µm coarse clays

Table 5. Total analyses of selected fractions as percentage of dry sample.

Samples	SiO$_2$	Al$_2$O$_3$	Fe$_2$O$_3$	MnO	MgO	CaO	Na$_2$O	K$_2$O	TiO$_2$	Σ
C, 10–20, 0.2 M	31.17	22.90	20.98	0.17	10.95	0.75	0.50	3.20	2.42	93.04
C, 10–20, 2 M	46.07	29.71	8.25	0.05	4.62	0.33	1.13	6.81	1.18	98.15
C, 1–2, M	40.16	28.09	10.40	0.06	5.78	0.19	1.12	6.07	1.08	92.95
Bw, 1–2, M	44.87	25.01	6.20	0.03	3.09	0.37	0.93	5.74	1.69	87.93
0.1–0.2, N	40.31	25.01	7.98	0.02	5.91	0.13	0.57	3.17	1.57	84.67
<0.1, N	39.87	24.64	9.41	0.02	5.64	0.12	0.54	2.83	1.57	84.64
Bh, 1–2, M	47.06	26.48	4.51	0.03	2.51	0.30	1.05	5.13	1.82	88.89
Bh, 0.1–0.2, N	41.16	26.81	8.01	0.02	2.57	0.26	0.79	4.11	1.63	85.36
<0.1, N	41.86	24.75	8.39	0.01	2.35	0.21	0.67	3.14	1.41	82.79
A1/E, 1–2, M	47.10	25.18	3.99	0.02	2.03	0.62	1.30	6.11	1.68	88.03
0.1–0.2, N	40.39	23.49	5.55	0.01	1.60	0.19	0.74	4.58	1.40	77.95
<0.1, N	42.37	25.01	5.90	0.01	2.05	0.23	0.81	4.71	1.35	82.44

in the A1/E horizon being a first stage of that transformation.

CONCLUSION

The clays in a podzolized soil developed in a chlorite-mica schist saprolite were produced by weathering of the pre-existing phyllosilicates. Physical fragmentation and mineralogical transformation were involved for the formation of soil clays. Chlorite and mica/chlorite mixed-layers in the larger particles of pre-existing phyllosilicates were more strongly affected by physical fragmentation than mica layers. A concentration of mica layers took place in the coarse clay fractions, as chloritic residues were accumulated in the fine clays. These were responsible for a typical XRD intergrade behavior, the interlayered contaminant being mostly hydroxy-Mg cations. Further mineralogical transformations induced by soil formation were the removal of the interlayered contaminant, leading to illite/smectite mixed-layer minerals as end products of the weathering processes.

REFERENCES

Adams, W. A. and Kassim, J. K. (1983) The origin of vermiculite developed from lower palaeozoic sedimentary rocks in Mid Wales: *Soil Sci. Soc. Am. J.* **47,** 316–320.

Bain, D. C. (1977) The weathering of chloritic minerals in some scottish soils: *J. Soil Sci.* **28,** 144–164.

Barnhisel, R. I. and Bertsch, P. M. (1989) Chlorites and hydroxy interlayered vermiculite and smectite: in *Minerals in Soil Environments:* 2nd ed., J. B. Dixon and S. B. Weed, eds., Soil Sci. Soc. Am., Madison, Wisconsin, 729–788.

Borchardt, G. (1989) Smectites: in *Minerals in Soil Environments:* 2nd ed., J. B. Dixon and S. B. Weed, eds., Soil Sci. Soc. Am., Madison, Wisconsin, 675–727.

Caillère, S. and Hénin, S. (1960) Relationship between the crystallochemical constitution of phyllites and their dehydration temperature application in the case of chlorites: *Bull. Soc. Fr. Ceram.* **48,** 63–67.

Churchman, G. J. (1980) Clay minerals formed from micas and chlorite in some New Zealand soils: *Clay Miner.* **15,** 59–76.

DeConinck, F., van Ranst, E., and Jensen, W. (1983) Trioctahedral and dioctahedral chlorite in soils: Examples of a Dystrochrept (Corsica), a Cryorthod (Norway) and a Hapludalf (France): in *Pétrologie des Altérations et des Sols,* D. Nahon and Y. Noack, eds., Sciences Géologiques, Strasbourg, 74–84.

Douglas, L. A. (1967) Sodium citrate-dithionite induced alteration of biotite: *Soil Sci.* **103,** 191–195.

Douglas, L. A. (1989) Vermiculites: in *Minerals in Soil Environments:* 2nd ed., J. B. Dixon and S. B. Weed, eds., Soil Sci. Soc. Am., Madison, Wisconsin, 635–674.

Ghabru, S. K., Mermut, A. R., and St. Arnaud, R. J. (1990) Isolation and characterization of an iron-rich chlorite-like mineral from soil clays: *Soil Sci. Soc. Am. J.* **54,** 281–287.

Greene-Kelly, R. (1953) The identification of montmorillonoids in clays. *J. Soil Sci.* **4,** 233–237.

INRA (1992) *Référentiel Pédologique, Principaux Sols d'Europe:* INRA, Paris, 222 pp.

Jeanroy, E. (1972) Analyse totale des silicates naturels par spectrophotométrie d'absorption atomique. Application au sol et à ses constituants: *Chim. Anal.* **54,** 159–166.

Lanson, B. and Besson, G. (1992) Characterization of the end of smectite-to-illite transformation: Decomposition of X-ray patterns: *Clays & Clay Minerals* **40,** 40–52.

Makumbi, L. and Herbillon, A. J. (1972) Vermiculitisation expérimentale d'une chlorite: *Bull. Groupe Fr. Argiles* **XXIV,** 153–164.

Mehra, O. P. and Jackson, M. L. (1960) Iron oxide removal from soils and clays by a dithionite-citrate system buffered with sodium bicarbonate: *Clays & Clay Minerals* **7,** 317–327.

Proust, D., Eymery, J.-P., and Beaufort, D. (1986) Supergene vermiculitization of a magnesian chlorite: Iron and magnesium removal processes: *Clays & Clay Minerals* **34,** 572–580.

Reynolds, R. C. (1980) Interstratified clay minerals: in *Crystal Structures of Clay Minerals and Their X-ray Identification,* G. W. Brindley and G. Brown, eds., Miner. Soc., London, 249–359.

Reynolds, R. C. (1985) *Description of Program NEWMOD for the Calculation of the One-dimensional X-ray Diffraction Patterns of Mixed-layered Clays:* R. C. Reynolds, 8 Brook Road, Hanover, New Hampshire, 24 pp.

Righi, D. and Jadault, P. (1988) Improving soil clay minerals studies by high-gradient magnetic separation: *Clay Miner.* **23,** 225–232.

Righi, D. and Lorphelin, L. (1986) Weathering of silt and clay in soils of a toposequence in the Himalayas, Nepal: *Geoderma* **39,** 141–155.

Righi, D. and Lorphelin, L. (1987) The soils of a typical slope in the Himalayas (Nepal): Their main characteristics and distribution: *Catena* **14,** 533–551.

Righi, D. and Meunier, A. (1991) Characterization and genetic interpretation of clays in an acid brown soil (Dystrochrept) developed in a granitic saprolite: *Clays & Clay Minerals* **39,** 519–530.

Ross, G. J., Wang, C., Ozkan, A. I., and Rees, H. W. (1982) Weathering of chlorite and mica in a New Brunswick podzol developed on till derived from chlorite-mica schist: *Geoderma* **27,** 255–267.

Senkayi, A. L., Dixon, J. B., and Hossner, L. R. (1981) Transformation of chlorite to smectite through regularly interstratified intermediates: *Soil Sci. Soc. Am. J.* **45,** 650–656.

Stucki, J. W., Golden, D. C., and Roth, C. B. (1984) Effects of reduction and reoxidation of structural iron on the surface charge and dissolution of dioctahedral smectites: *Clays & Clay Minerals* **32,** 350–356.

Tamura, T. (1958) Identification of clay minerals from acid soils: *J. Soil Sci.* **9,** 141–147.

USDA (1986) *Clés de la taxonomy des sols:* Monographie technique n°13. Cornell University, Ithaca, New York, 347 pp.

Weed, S. B. and Bowen, L. H. (1990) High-gradient magnetic concentration of chlorite and hydroxy-interlayered minerals in soil clays: *Soil Sci. Soc. Am. J.* **54,** 274–280.